

# Orbital magnetization of the electron gas on a two-dimensional kagomé lattice under a perpendicular magnetic field

Zhigang Wang,<sup>1</sup> Zi-Gang Yuan,<sup>2,3</sup> Zhen-Guo Fu,<sup>1,2</sup> Shu-Shen Li,<sup>2</sup> and Ping Zhang<sup>1,4,\*</sup>

<sup>1</sup>*LCP, Institute of Applied Physics and Computational Mathematics,  
P.O. Box 8009, Beijing 100088, People's Republic of China*

<sup>2</sup>*State Key Laboratory for Superlattices and Microstructures,  
Institute of Semiconductors, Chinese Academy of Sciences,  
P. O. Box 912, Beijing 100083, People's Republic of China*

<sup>3</sup>*College of Science, Beijing University of Chemical Technology,  
Beijing 100029, People's Republic of China*

<sup>4</sup>*Center for Applied Physics and Technology,  
Peking University, Beijing 100871, People's Republic of China*

## Abstract

The orbital magnetization of the electron gas on a two-dimensional kagomé lattice under a perpendicular magnetic field is theoretically investigated. The interplay between the lattice geometry and magnetic field induce nontrivial  $k$ -space Chern invariant in the magnetic Brillouin zone, which turns to result in profound effects on the magnetization properties. We show that the Berry-phase term in the magnetization gives a paramagnetic contribution, while the conventional term brought about by the magnetic response of the magnetic Bloch bands produces a diamagnetic contribution. As a result, the superposition of these two components gives rise to a delicate oscillatory structure in the magnetization curve when varying the electron filling factor. The relationship between this oscillatory behavior and the Hofstadter energy spectrum is revealed by selectively discussing the magnetization and its two components at the commensurate fluxes of  $f=1/4$ ,  $1/3$ , and  $1/6$ , respectively. In particular, we reveal as a typical example the fractal structure in the magnetic oscillations by tuning the commensurate flux around  $f=1/4$ . The finite-temperature effect on the magnetization is also discussed.

PACS numbers: 73.20.At, 71.10.Ca, 72.15.Gd

---

\*Author to whom correspondence should be addressed. Electronic address: zhang\_ping@iapcm.ac.cn

## I. INTRODUCTION

Over the past three decades, the orbital dynamics of two-dimensional (2D) electrons coupled to a uniform perpendicular magnetic field has been a subject of special interest in condensed matter physics. Great attention has been paid to investigate the well-known Hofstadter butterfly-like diagram, a remarkable intricate, detailed, and self-similar feature for the subband spectrum of single-particle eigenenergies, in different 2D structures such as square [1], triangular [2], honeycomb [3], and kagomé lattices [4], lateral superlattices [5], superstructures with flat bands [6], quasiperiodic tilings [7], fractal networks [8], and rhombus tilings [9]. This magnetic-field-induced frustration in 2D structures, caused by the competition between the periodic potential imposed by the lattice structure and the length scale provided by the magnetic field, is the headstream of rich and novel physical phenomena in these 2D systems. Among them the orbital magnetization is a very interesting one and needs to be paid special attention due to its intrinsic relationship with the unique topological structure brought about by the interplay between the special lattice geometry and magnetic subbands. Unfortunately, to date, there are very scarce studies [10, 11] in literature that devote to enlightening this revealing relationship.

Motivated by this observation, in this paper, we study the orbital magnetization properties of the electron gas on a two-dimensional kagomé lattice under a perpendicular magnetic field. Since our attention is solely on the orbital character in magnetization brought about by the interplay between the kagomé lattice structure and the magnetic field, thus unlike most of previous work, the kagomé lattice considered in this paper is spin nonmagnetic in itself, namely, no spin structure is exposed in the absence of the external magnetic field. The nonmagnetic kagomé lattice structure has been either fabricated by modern patterning techniques [12, 13] or observed in reconstructed semiconductor surfaces [14]. In the former case, remarkably, the electron filling factor (namely, the Fermi energy) can be readily controlled by applying a gate voltage [15]. Our lattice model is free from the constraint imposed on the  $\mathbf{k}\cdot\mathbf{p}$  approximation used in the extensively studied GaAs two-dimensional electron gas (2DEG), in which the  $\mathbf{k}\cdot\mathbf{p}$  Hamiltonian is only valid around the  $\Gamma$  point in the Brillouin zone (BZ). In contrast, our lattice model allows for any electron filling, which result in various Fermi-surface topologies in the magnetic BZ, which in turn, as will be shown below, produces profound effects on the orbital magnetization properties and the related transport

phenomenon.

The orbital magnetization for Bloch electrons combines two terms [10, 16], one is the conventional orbital magnetic moment to characterize the magnetic response of the single-particle energy spectrum, and the other is a Berry-phase correction. These two terms play different roles in metallic and insulating regions [17, 18]. By varying the Fermi energy, we obtain the follows: (i) Both the magnitudes of these two terms increase (decrease) with increasing (decreasing) the Fermi energy in metallic regions; (ii) In insulating regions the conventional term keeps a constant unchanged value (quantum step), while the Berry-phase linearly varies with the Fermi energy with a slope proportional to the system's Hall conductance; (iii) A general fractal structure may occur in the orbital magnetization curve (as a function of the Fermi energy) by tuning the commensurate flux.

The rest of this paper is organized as follows. In Sec. II we give the Hofstadter spectrum of the kagomé lattice by diagonalizing the corresponding tight-binding Hamiltonian in an external magnetic field. In Sec. III the orbital magnetization and its two components are systematically discussed by varying various system parameters. A summary is given in Sec. IV.

## II. KAGOMÉ LATTICE IN A MAGNETIC FIELD

The kagomé lattice is a two-dimensional periodic array of corner-sharing triangles with three sites per unit cell, as illustrated in Fig. 1. Here  $a$  is the triangle edge length (we set it as the length unit in the following), and  $A$ ,  $B$ , and  $C$  denote the three sites in a unit cell. Let us begin with the tight-binding Hamiltonian for the spinless electrons on the kagomé lattice with zero magnetic field ( $\mathbf{B}=0$ ), which is given by

$$\mathcal{H} = t \sum_{\langle i,j \rangle} c_i^\dagger c_j, \quad (1)$$

where  $t$  is hopping amplitude between the nearest-neighbor link  $\langle i, j \rangle$  and  $c_i^\dagger$  ( $c_i$ ) is the creation (annihilation) operator of an electron on lattice  $i$ . Hamiltonian (1) can be diagonalized in the momentum space as

$$\mathcal{H} = t \sum_{\mathbf{k}} \Psi_{\mathbf{k}}^\dagger H(\mathbf{k}) \Psi_{\mathbf{k}}, \quad (2)$$

where  $\Psi_{\mathbf{k}}=(c_{\mathbf{k}A}, c_{\mathbf{k}B}, c_{\mathbf{k}C})^T$  is the three-component electron field operator. Each component of  $\Psi_{\mathbf{k}}$  is the Fourier transform of  $c_i$ , i.e.,

$$c_{\mathbf{k}s} = \sum_{mns} c_{mns} e^{i\mathbf{k}\cdot\mathbf{r}_{mns}}, \quad (3)$$

where we have changed notation  $i \rightarrow (mns)$  by using  $(mn)$  to label the kagomé unit cells and  $s$  to label the three sites in a unit cell.  $H(\mathbf{k})$  is given by

$$H(\mathbf{k}) = \begin{pmatrix} 0 & p_{\mathbf{k}}^1 & p_{\mathbf{k}}^3 \\ p_{\mathbf{k}}^1 & 0 & p_{\mathbf{k}}^2 \\ p_{\mathbf{k}}^3 & p_{\mathbf{k}}^2 & 0 \end{pmatrix}, \quad (4)$$

where  $p_{\mathbf{k}}^i=2 \cos(\mathbf{k} \cdot \mathbf{a}_i)$  and  $\mathbf{a}_1=(-1/2, -\sqrt{3}/2)$ ,  $\mathbf{a}_2=(1, 0)$ , and  $\mathbf{a}_3=(-1/2, \sqrt{3}/2)$  represent the displacements in a unit cell from the  $A$  to  $B$  site, from the  $B$  to  $C$  site, and from the  $C$  to  $A$  site, respectively. In this notation, the first BZ is a hexagon with the corners of  $\mathbf{K}=\pm(2/3)\mathbf{a}_1$ ,  $\pm(2/3)\mathbf{a}_2$ , and  $\pm(2/3)\mathbf{a}_3$ .

In the presence of a magnetic field ( $\mathbf{B} \neq 0$ ), the hopping term of the tight-binding Hamiltonian (1) is modified by phase factors from the vector potential  $\mathbf{A}$ ,

$$t \rightarrow t e^{i\gamma_{ij}} \quad (5)$$

where  $\gamma_{ij}$  is the phase factor (the well known Peierls phase) between sites  $j$  and  $i$ :

$$\gamma_{ij} = \frac{2\pi}{\Phi_0} \int_j^i \mathbf{A} \cdot d\mathbf{l} \quad (6)$$

with  $\Phi_0=h/e$  being the flux quantum.

One can take different gauge potential  $\mathbf{A}$  mathematically to satisfy the physical confinement  $\nabla \times \mathbf{A}=\mathbf{B}$ . However, the flux through one unit cell is only linearly dependent on the external magnetic field  $\mathbf{B}$ , and has no relation with the choice of the gauge potential  $\mathbf{A}$ . So, it is convenient to measure the magnetic field in units of the flux quantum per elementary triangular plaquette of the kagomé lattice. After a simple algebraic calculation, one obtains the flux through one triangle is  $\Phi=\sqrt{3}B/4$ . Thus we can define a parameter, called the filling ratio  $f$ , as the fraction of a flux quantum through each triangle, i.e,  $f=\Phi/\Phi_0=\sqrt{3}eB/4h$  [4]. The total flux through a unit cell of the kagomé lattice is then given as  $8f\Phi_0$ .

When  $f$  is a rational number that can be written as  $f=p/q$ , where  $p$  and  $q$  are integers with no common factors, the total flux through  $q$  triangular plaquette of the kagomé lattice

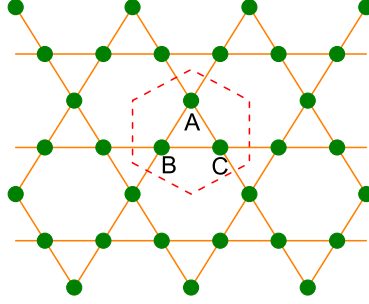


FIG. 1: (Color online). Schematic picture of the 2D kagomé lattice with bond length  $a$ . The dashed line represents the Wigner-Seitz unit cell, which contains three independent sites ( $A$ ,  $B$ , and  $C$ ).

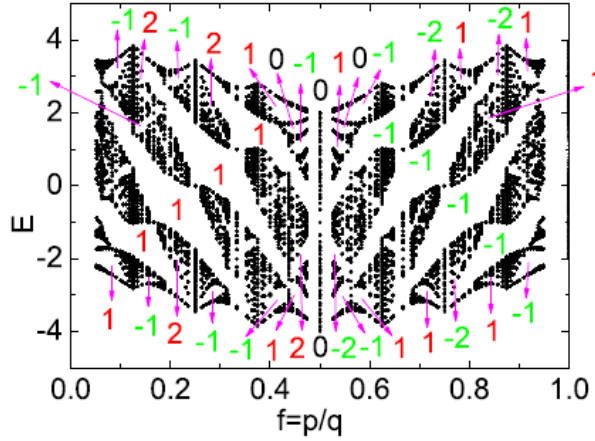


FIG. 2: (Color online). Hofstadter butterfly-like spectrum of the 2D Kagomé lattice. The numbers recorded in gaps represent the Hall conductance of this system in units of  $e^2/h$  when the Fermi energy lies in these gaps.

is an integer multiple of  $\Phi_0$ . In this case, the Hamiltonian (1) should be diagonalized in a “magnetic” unit cell, which contains  $q$  plaquette in order to guarantee  $\mathbf{k}$  being good quantum numbers. As a result, the magnetic Brillouin zone (MBZ) is  $q$  times smaller than the usual BZ. Furthermore, because of the magnetic translation symmetry, the MBZ has exactly a  $q$ -fold degeneracy. For convenience we take the gauge potential as  $\mathbf{A}=B(-\frac{1}{2}(-\sqrt{3}x+y), \frac{1}{2}(x-\frac{1}{\sqrt{3}}y), 0)$ . Under this gauge, the Peierls phases, which reflect the information about the external magnetic field, are only related to  $n$  and have nothing with  $m$ . The Hamiltonian of the kagomé lattice now can be diagonalized in the momentum space as the following  $3q \times 3q$

matrix,

$$\begin{aligned}
H(\mathbf{k}) = & \sum_{n=0}^{q-1} \left[ h_n^{BA} c_{nB}^\dagger c_{nA} + h_n^{BA*} c_{nB}^\dagger c_{nA} \right. \\
& + h_n^{CB} c_{nC}^\dagger c_{nB} + \exp(-i4\pi f) h_{n+1}^{CB*} c_{nC}^\dagger c_{n+1B} \\
& \left. + h_n^{AC} c_{nA}^\dagger c_{nC} + h_n^{AC*} c_{n+1A}^\dagger c_{nC} + \text{H.c.} \right], \tag{7}
\end{aligned}$$

where

$$\begin{aligned}
h_n^{BA} &= t \exp(-i\mathbf{k} \cdot \mathbf{a}_1) \exp \left[ -i8\pi f \left( n - \frac{1}{6} \right) \right], \\
h_n^{CB} &= t \exp(-i\mathbf{k} \cdot \mathbf{a}_2) \exp \left[ i8\pi f \left( n + \frac{1}{12} \right) \right],
\end{aligned}$$

and

$$h_n^{AC} = t \exp(-i\mathbf{k} \cdot \mathbf{a}_3).$$

With the above Hamiltonian (7), it is straightforward to obtain the Hofstadter butterfly-like energy spectrum of the kagomé lattice, which is shown in Fig. 2.

From Fig. 2, one can easily observe three symmetries of this Hofstadter butterfly-like spectrum of the kagomé lattice [4]: (i) The spectrum at  $f$  is the same as that at  $f + j$  with  $j$  any integer; (ii) The spectrum is also unchanged on changing  $f$  to  $-f$ , because if there is an eigenstate with energy  $\epsilon$  for field  $f$ , then the corresponding complex conjugate of this eigenstate is also an eigenstate with the same energy  $\epsilon$  for field  $-f$ ; (iii) The spectrum is inverted when the field  $f$  changes to  $f + 1/2$ . Thus the highest-energy states for field near  $f=1/2$  are equivalent to the lowest-energy states near zero field.

### III. THE PROPERTIES OF THE ORBITAL MAGNETIZATION

To obtain the orbital magnetization of the kagomé lattice in an external magnetic field and with finite temperature, let us first write down the single-particle free energy as follows [16]:

$$F = -\frac{1}{\beta} \sum_n \int_{\text{MBZ}} d^2\mathbf{k} \left[ 1 + \frac{e}{\hbar} \mathbf{B} \cdot \Omega_n(\mathbf{k}) \right] \ln[1 + e^{\beta(\mu - \epsilon_{n\mathbf{k}})}]. \tag{8}$$

Here,  $\Omega_n(\mathbf{k})$  is the Berry curvature of electronic Bloch states defined by  $\Omega_n(\mathbf{k}) = i \langle \nabla_{\mathbf{k}} u_{n\mathbf{k}} | \times | \nabla_{\mathbf{k}} u_{n\mathbf{k}} \rangle$  with  $|u_{n\mathbf{k}}\rangle$  being the periodic part of Bloch wave for the  $n$ th band. Its

integral over the MBZ gives the topological invariant, namely, the Chern number  $C_n = -\frac{1}{2\pi} \int_{\text{MBZ}} d^2\mathbf{k} \Omega_n(\mathbf{k})$ . The sum of Chern numbers over the integer occupied bands gives the quantized Hall conductance in unit of  $e^2/h$  (see numbers in Fig. 2).  $\mu$  in Eq. (8) is the electron chemical potential,  $\beta=1/k_B T$ , and  $\epsilon_{n\mathbf{k}}$  is the magnetic band energy. When the field varies by an infinitesimal quantity, i.e., from  $\mathbf{B}$  to  $\mathbf{B}+\delta\mathbf{B}$ , then the magnetic band energy can be linearly expanded as  $\epsilon_{n\mathbf{k}}(\mathbf{B}+\delta\mathbf{B}) = \epsilon_{n\mathbf{k}}(\mathbf{B}) - m_{n\mathbf{k}}(\mathbf{B}) \cdot \delta\mathbf{B}$ , where  $m_{n\mathbf{k}}$  is the conventional crystal orbital magnetic moment defined by  $\bar{m}_{n\mathbf{k}} = -i(e/2\hbar) \langle \nabla_{\mathbf{k}} u_{n\mathbf{k}} | \times [H(\mathbf{k}) - \epsilon_{n\mathbf{k}}] | \nabla_{\mathbf{k}} u_{n\mathbf{k}} \rangle$  in the MBZ. The magnetization is then given by the field derivative at fixed temperature and chemical potential,  $\mathcal{M} = -(\partial F/\partial \mathbf{B})_{\mu, T}$ , with the result

$$\begin{aligned} \mathcal{M} &= \sum_n \int_{\text{MBZ}} d^2\mathbf{k} \mathbf{m}_n(\mathbf{k}) f_n(\mathbf{k}) \\ &+ \frac{1}{\beta} \sum_n \int_{\text{MBZ}} d^2\mathbf{k} \frac{e}{\hbar} \Omega_n \ln [1 + e^{\beta(\mu - \epsilon_{n\mathbf{k}})}] \\ &\equiv \mathbf{M}_c + \mathbf{M}_\Omega, \end{aligned} \quad (9)$$

where  $f_n(\mathbf{k})$  is the equilibrium Fermi-Dirac distribution function for  $n$ th magnetic Bloch band. The first term in Eq. (9) is just a statistical sum of the orbital magnetic moments of the carriers originating from the self-rotation of the carrier wave packet [19, 20], thus we call this term the conventional part  $\mathbf{M}_c$  of the orbital magnetization. Whereas the second term  $\mathbf{M}_\Omega$  is the Berry-phase correction to the orbital magnetization. This term is of topological nature. Interestingly, it is this Berry-phase term that eventually enters the transport current [21]. At zero temperature the general expression (9) reduces to [10, 16, 22]

$$\mathcal{M} = \sum_n \int_{\text{MBZ}}^{\mu_0} d^2\mathbf{k} \left[ \mathbf{m}_n(\mathbf{k}) + \frac{e}{\hbar} \Omega_n(\mathbf{k}) (\mu_0 - \epsilon_{n\mathbf{k}}) \right], \quad (10)$$

where the upper limit means that the integral is over magnetic Bloch states with energies below the Fermi energy  $\mu_0$ .

Now with the help of the knowledge on the magnetic energy spectrum obtained from diagonalizing the Hamiltonian (7), we can numerically obtain the magnetization  $\mathcal{M}$  for different field  $f$ . First, let us consider the case with field  $f=1/4$ . In this case, the energy spectrum splits into three bands between which there are two band gaps with the same gap width  $\Delta=1.74$  (see Fig. 3(a)). The middle band collapse into a plane in the MBZ. The calculated zero-temperature magnetization  $\mathcal{M}$  is plotted in Fig. 3(b). From this figure, one can find that with the Fermi energy  $\mu_0$  increases from  $-3.26$ , the lower band begins to be

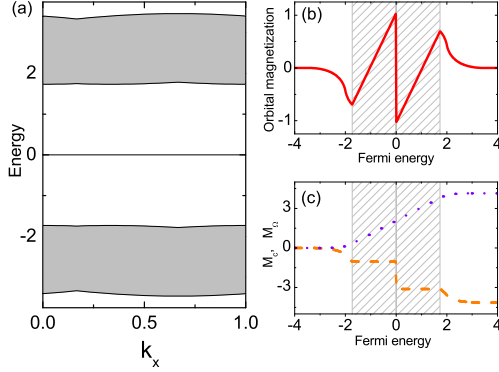


FIG. 3: (Color online). (a) Energy spectrum of the 2D kagomé lattice with a field  $f=1/4$ . The shadow areas are the energy bands. The corresponding magnetization  $\mathcal{M}$  and its two components are respectively drawn in (b) and (c) as functions of the Fermi energy  $\mu_0$ . The shaded areas in (b) and (c) are the insulating regions. The dashed and dotted lines in (c) represent  $M_c$  and  $M_\Omega$ , respectively.

occupied and  $\mathcal{M}$  begins to decrease from 0. When  $\mu_0$  increases to  $-1.74$ , the lower band is fully occupied and the magnetization decreases to  $-0.7e/h$ . When continue increasing  $\mu_0$ , the system enters the first insulating region. The magnetization then linearly increases with the Fermi energy until the middle band is occupied ( $\mu_0=0^-$ , at this time  $\mathcal{M}=1.03e/h$ ). When further increasing the Fermi energy, the system immediately comes into the second insulating region and the magnetization jumps down to  $-1.03e/h$  and then linearly increases up to  $0.7e/h$  until the upper band begins to be occupied ( $\mu_0=1.74$ ). Then the magnetization decreases to 0 with the Fermi energy going through the upper band.

As shown in Refs. [17, 18], the totally different behavior of the magnetization in the metallic and insulating regions is due to the different roles  $M_c$  and  $M_\Omega$  play in these two regions. For further illustration, we show in Fig. 3(c)  $M_c$  (dashed line) and  $M_\Omega$  (dotted line) as functions of the Fermi energy, their sum gives  $\mathcal{M}$  in Fig. 3(b). One can see that overall  $M_c$  and  $M_\Omega$  have opposite contributions to  $\mathcal{M}$ , which implies that these two parts carry opposite-circulating currents. In each insulating regime the conventional term  $M_c$  keeps a constant, which is due to the fact that the upper limit of the  $k$ -integral of  $m_n(\mathbf{k})$  is invariant as the chemical potential varies in the gap. In the metallic region, however, since the occupied states varies with the Fermi energy, thus  $M_c$  also varies with  $\mu_0$ , resulting in a decreasing slope shown in Fig. 3(c). The Berry phase term  $M_\Omega$  also displays different



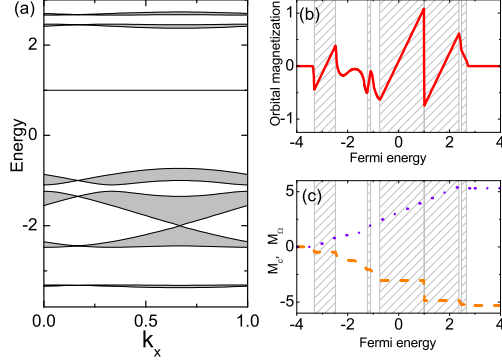


FIG. 4: (Color online). Energy spectrum and orbital magnetization for  $f=1/3$ .

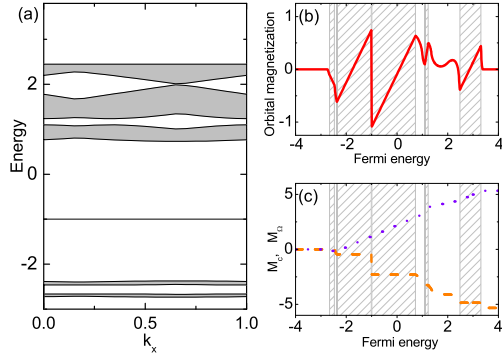


FIG. 5: (Color online). Energy spectrum and orbital magnetization for  $f=1/6$ .

behavior between insulating and metallic regions. In the insulating region,  $M_\Omega$  linearly increases with  $\mu_0$ , as is expected from Eq. (10). The slope of the Berry-phase correction term in insulating regions is proportional to the system's Hall conductance. In the metallic region, however, this term sensitively depends on the topological property of the band in which the chemical potential is located. On the whole the comparison between Fig. 3(b) and Fig. 3(c) shows that the metallic behavior of  $\mathcal{M}$  is dominated by its conventional term  $M_c$ , while in the insulating regime  $M_\Omega$  plays a main role in determining the behavior of  $\mathcal{M}$ .

Now let us consider more complex cases, for example, with a field  $f=1/3$  and with a field  $f=1/6$ . In these two case, there are more energy bands and gaps appearing in the energy spectrum [see Figs. 4(a) and 5(a)]. Figures 4(b) and 4(c), and Figs. 5(b) and 5(c), for  $f=1/3$  and  $f=1/6$ , respectively, plot the magnetization  $\mathcal{M}$  and its two components as functions of  $\mu_0$ . Clearly from these figures, one can observe a similar variation of the magnetization by changing the electron's fillings (the Fermi energy  $\mu_0$ ). Comparing the case of  $f=1/3$  [Fig.

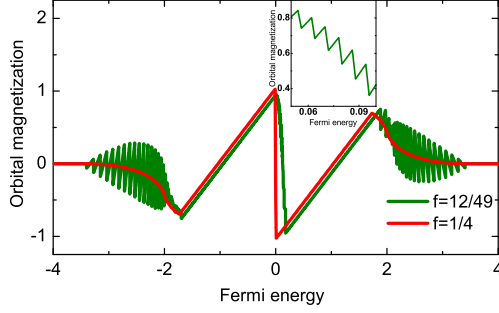


FIG. 6: (Color online). The magnetization  $\mathcal{M}$  as a function of the Fermi energy  $\mu_0$  in the fields  $f=1/4$  and  $f'=12/49$ . The inset is the enlarged vision of the magnetization  $\mathcal{M}$  at  $f'=12/49$  when the Fermi energy varies between 0.05 and 0.1.

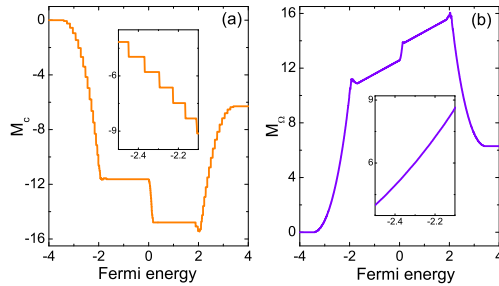


FIG. 7: (Color online). The two components of the magnetization  $\mathcal{M}$  as functions of the Fermi energy  $\mu_0$  at  $f=12/49$ .

4(a)] to the case of  $f=1/6$  [Fig. 5(a)], one can find that the orbital magnetization in these two fields have a relation

$$\mathcal{M}(f = \frac{1}{6}, \mu_0) = \mathcal{M}(f = \frac{1}{3}, -\mu_0). \quad (11)$$

This conclusion is a combined exhibition of the above mentioned symmetries (ii) and (iii) in the Hofstadter energy spectrum.

We have known that the topology of the energy spectrum of the 2D lattice system arises from the competition between the periodic potential-induced level broadening and the magnetic field-induced level discretization. Once the external magnetic field changes, the topology of the energy spectrum also changes, which results in the simultaneous prominent variation in the magnetization of the 2D system. The above discussions on the magnetization for different fields  $f=1/4$ ,  $1/3$  and  $1/6$  are typical examples. Now a question is put forward:

If there is a very small perturbation  $\delta f$  to the field  $f$ , then how about the change in the magnetization? The answer is the occurrence of fractal structure in the magnetic de Haas-van Alphen (dHvA) oscillations, which is very important for the experimental measurement of the Fermi surface topology.

Now we investigate this fractal structure in the magnetic oscillations for the present system. For convenience and simplicity, we choose the field  $f=1/4$  and the perturbation  $\delta f=-1/196$  ( $f'=f+\delta f=12/49$ ). The calculated magnetization  $\mathcal{M}$  at the fields  $f$  and  $f'$  are plotted in Fig. 6. From Fig. 6 one can observe the following features: (i) In the insulating region, the magnitudes of the magnetization  $\mathcal{M}$  have little difference at the fields  $f$  and  $f'$ . The perturbation  $\delta f$  is more small, more little in the changes of the magnetization  $\mathcal{M}$ ; (ii) In the metallic regions at the field  $f$ , however, there are dHvA oscillations appearing in the magnetization  $\mathcal{M}$  at the field  $f+\delta f$ . The perturbation  $\delta f$  is more small, the magnetization oscillates more rapidly; (iii) The collapsed middle band originally at field  $f=1/4$  now spreads at  $f'=12/49$ . And in this middle band there are also dHvA oscillations appearing in the orbital magnetization. To see this fractal feature more clearly, we enlarge the magnetization in the inset in Fig. 6; (iv) There are similar variations in the two components of  $\mathcal{M}$  (see Fig. 7). In the insulating regions at  $f=1/4$ , there are little difference in the conventional and Berry-phase terms. However, both terms exhibit different behaviors in the metallic regions. While the Berry-phase term has little difference at different fields as it in the insulating regions, there are many quantum steps appearing in the conventional term at  $f'=12/49$ . The reason for these quantum steps appearing in the conventional magnetization is that the topology of the energy spectrum at the field  $f'=f+\delta f$  is different from that at the field  $f$ . When the external field  $f$  changes to  $f+\delta f$ , the eigenbands at the field  $f$  split into lots of subbands. The perturbation  $\delta f$  is more small, the number of the splitting subbands is more large. Because the upper limit of the  $k$ -integral of  $m_n(\mathbf{k})$  is invariant as the Fermi level  $\mu_0$  varies in the subgap, then the conventional term in the subgap keeps a constant, which is the reason for the quantum step appearing in the conventional term. On the other hand, the integral of the Berry-phase term intimately depends on the Fermi level and has no such relation with the energy gaps (or bands). That results in the little difference in the Berry-phase term at different fields. So, when one changes the electron's fillings through these splitting bands, the total magnetization then exhibits the fractal structure in the magnetic dHvA oscillations.

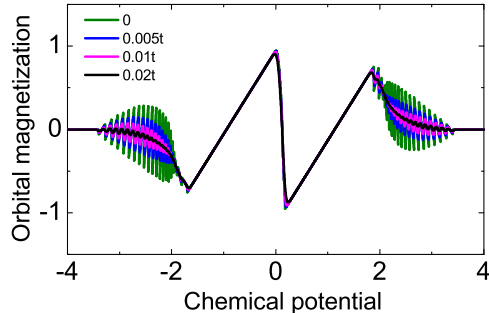


FIG. 8: (Color online). The magnetization  $\mathcal{M}$  as a function of the electron chemical potential at the field  $f=12/49$  with different temperatures.

In the above discussions on the orbital magnetization of the 2D kagomé lattice, we have concentrated on the zero-temperature limit and omitted finite-temperature effect. Now let us briefly consider the more realistic cases in which the finite-temperature effect is included. Figure 8 plots the orbital magnetization at the field  $f=12/49$  with different temperatures  $k_B T=0, 0.005, 0.01, \text{ and } 0.02$ , respectively. From Fig. 8, one can find that the magnetic oscillations are suppressed by thermal broadening.

#### IV. SUMMARY

In summary, we have theoretically investigated the orbital magnetization of a 2D kagomé lattice in a perpendicular magnetic field. Here, the orbital magnetization includes a conventional term and a Berry-phase term, which play different roles in metallic and insulating regions. As examples, we have carefully discussed the orbital magnetization and its two components at the fields  $f=1/4, 1/3, \text{ and } 1/6$ , respectively. By varying the Fermi energy  $\mu_0$ , we have obtained the following results: (i) The conventional term and the Berry-phase term give the opposite contributions, with their magnitudes increasing (decreasing) with increasing (decreasing) the Fermi energy in metallic regions; (ii) The conventional term keeps unchanged in insulating regions; (iii) The slope of the Berry-phase term in insulating regions is proportional to the system's Hall conductance. When the flux is applied near a commensurate one (for example,  $1/4$ ), the magnetic dHvA oscillations develop a fractal structure, i.e., the orbital magnetization rapidly oscillates when the Fermi energy varies through the split subbands. The finite-temperature effect has also been shown to suppress the oscillating

amplitude of the orbital magnetization.

### Acknowledgments

This work was supported by NSFC under Grants No. 90921003, No. 10904005, No. 60776061 and No. 60776063, and by the National Basic Research Program of China (973 Program) under Grants No. 2009CB929103 and No. 2009CB929300.

- 
- [1] D. R. Hofstadter, Phys. Rev. B **14**, 2239 (1976); G. H. Wannier, Phys. Status Solidi B **88**, 757 (1978); G. H. Wannier, G. M. Obermair, and R. Ray, Phys. Status Solidi B **93**, 337 (1979).
  - [2] F. H. Claro and G. H. Wannier, Phys. Rev. B **19**, 6068 (1979).
  - [3] R. Rammal, J. Phys. (Paris) **46**, 1345 (1985).
  - [4] Y. Xiao, V. Pelletier, P. M. Chaikin, and D. A. Huse, Phys. Rev. B **67**, 104505 (2003).
  - [5] M. A. Andrade Neto and P. A. Schulz, Phys. Rev. B **52**, 14093 (1995).
  - [6] H. Aoki, M. Ando, and H. Matsumura, Phys. Rev. B **54**, R17296 (1996).
  - [7] A. Behrooz, M. J. Burns, H. Deckman, D. Levine, B. Whitehead, and P. M. Chaikin, Phys. Rev. Lett. **57**, 368 (1986); K. Springer and D. van Harlingen, Phys. Rev. B **36**, 7273 (1987); H. Schwabe, G. Kasner, and H. Böttger, Phys. Rev. B **56**, 8026 (1997).
  - [8] B. Douçot, W. Wang, B. Pannetier, P. Rammal, A. Varelle, and D. Henry, Phys. Rev. Lett. **57**, 1235 (1986); J. M. Gordon, A. M. Goldman, J. Maps, D. Costello, R. Tiberio, and B. Whitehead, Phys. Rev. Lett. **56**, 2280 (1986); Q. Niu and F. Nori, Phys. Rev. B **39**, 2134 (1989).
  - [9] J. Vidal, R. Mosseri, and B. Douçot, Phys. Rev. Lett. **81**, 5888 (1998).
  - [10] O. Gat and J. E. Avron, Phys. Rev. Lett. **91**, 186801 (2003).
  - [11] O. Gat and J. E. Avron, New J. Phys. **5**, 441 (2003).
  - [12] P. Mohan, F. Nakajima, M. Akabori, J. Motohisa, and T. Fukui, Appl. Phys. Lett. **83**, 689 (2003); P. Mohan, J. Motohisa, and T. Fukui, Appl. Phys. Lett. **84**, 2664 (2004).
  - [13] M. J. Higgins, Y. Xiao, S. Bhattacharya, P. M. Chaikin, S. Sethuraman, R. Bojko, and D. Spencer, Phys. Rev. B **61**, R894 (2000); Y. Xiao, D. A. Huse, P. M. Chaikin, M. J. Higgins, S. Bhattacharya, and D. Spencer, *ibid.* **65**, 214503 (2002).

- [14] S. Y. Tong, G. Xu, W. Y. Hu, and M. W. Puga, *J. Vac. Sci. Technol. B* **3**, 1076 (1985).
- [15] K. Shiraishi, H. Tamura, and H. Takayanagi, *Appl. Phys. Lett.* **78**, 3702 (2001).
- [16] D. Xiao, J. Shi, and Q. Niu, *Phys. Rev. Lett.* **95**, 137204 (2005).
- [17] Z. Wang and P. Zhang, *Phys. Rev. B* **76**, 064406 (2007).
- [18] Z. Wang, P. Zhang, and J. Shi, *Phys. Rev. B* **76**, 094406 (2007).
- [19] M.-C. Chang and Q. Niu, *Phys. Rev. B* **53**, 7010 (1996).
- [20] G. Sundaram and Q. Niu, *Phys. Rev. B* **59**, 14915 (1999).
- [21] D. Xiao, Y. Yao, Z. Fang, and Q. Niu, *Phys. Rev. Lett.* **97**, 026603 (2006).
- [22] T. Thonhauser, D. Ceresoli, D. Vanderbilt, and R. Resta, *Phys. Rev. Lett.* **95**, 137205 (2005).